Journal of Power Sources 251 (2014) 402–410

Contents lists available at ScienceDirect

Journal of Power Sources

journal homepage: www.elsevier.com/locate/jpowsour

Activity, short-term stability (poisoning tolerance) and durability of carbon supported Pt–Pr catalysts for ethanol oxidation

Patricia G. Corradini [a], Ermete Antolini [b], Joelma Perez [a,*]

[a] Instituto de Química de São Carlos, USP, C. P. 780, São Carlos, SP 13560-970 São Paulo, Brazil
[b] Scuola di Scienza dei Materiali, Via 25 aprile 22, Cogoleto, 16016 Genova, Italy

HIGHLIGHTS

- Pt–Pr/C electrocatalysts are reported in this work.
- We evaluated the activity for carbon monoxide and ethanol oxidation.
- Short-term stability and durability were compared to Pt/C and Pt–Sn/C catalysts.
- The ethanol oxidation was favoured through the pathway at lower potential.

GRAPHICAL ABSTRACT

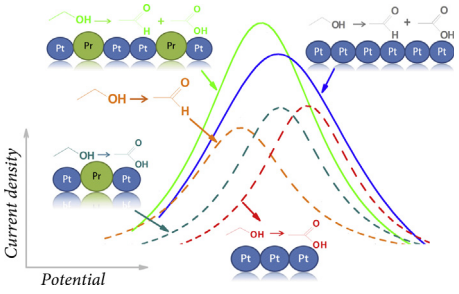

ARTICLE INFO

Article history:
Received 15 October 2013
Received in revised form
20 November 2013
Accepted 22 November 2013
Available online 4 December 2013

Keywords:
Pt–Pr/C catalysts
Ethanol oxidation
Stability
Fuel cell

ABSTRACT

Pt–Pr/C electrocatalysts were prepared by a modified formic acid method, and their activity for carbon monoxide and ethanol oxidation, their short term stability and durability were compared to that of commercial Pt/C and Pt–Sn/C (3:1) catalysts. By derivative voltammetry (DV) it was found that ethanol electro-oxidation takes place by two main pathways at different potentials. It was observed that, in the presence of Pr, ethanol electro-oxidation takes place mostly through the pathway at lower potential, which is the most interesting for fuel cell application. The Pt–Pr/C catalysts were less tolerant to poisoning by ethanol oxidation intermediate species than Pt/C. Durability test by a repetitive potential cycling under Ar atmosphere revealed a good structural stability of Pt–Pr/C catalysts. A repetitive potential cycling under CO atmosphere carried out on the Pt–Pr/C (1:1) catalyst, instead, indicated a structural change, likely by formation of a core–shell structure.

1. Introduction

Recently, the use of rare earths in low-temperature fuel cells has been reported. [1] Rare earth-based materials can play different roles in low-temperature fuel cells fuelled with hydrogen or low molecular weight alcohols, as catalysts and co-catalysts in both anode and cathode. Among rare earths, the use of cerium in low-temperature fuel cells was mostly investigated. Many studies have been addressed to the effect of the addition of CeO_2 to Pt/C [2–15] on electrochemical oxidation of methanol [2–13,15] and ethanol [2,3,7,14,15], in both acid [4–13] and alkaline media [2,3,14]. Generally, the Pt–CeO_2/C catalysts in the optimum Pt–CeO_2 molar ratio, varying in a wide range from 0.9 to 3.9, showed improved activity and stability in comparison to Pt/C [1]. The promoting action of CeO_2 on the catalytic activity of Pt was overall attributed to the high oxygen storage capacity of CeO_2, making easier the oxidation of adsorbed CO, and the high dispersion of Pt over CeO_2. The group at IPEN, Brazil, investigated the effect of the addition of a series of Ln to Pt/C [16], PtRu/C [17] and PtSn/C [18] on ethanol oxidation. In all cases the Ln-containing catalysts showed higher activity compared to the parent catalyst. Notwithstanding the tetravalent oxidation state of praseodymium is known to be a strong oxidizing agent [19], few studies were addressed to ethanol oxidation on Pt–Pr catalysts.

* Corresponding author. Tel.: +55 16 33739926; fax: +55 16 33739952.
E-mail address: jperez@iqsc.usp.br (J. Perez).

0378-7753/$ – see front matter © 2013 Elsevier B.V. All rights reserved.
http://dx.doi.org/10.1016/j.jpowsour.2013.11.078

[20,21] Nanopowders of the Laves-phase intermetallic compounds $LnPt_2$ (Ln = Ce, Pr) were utilized to exploit the strong oxidizing power of tetravalent lanthanides in an anode electrocatalyst. [20] Steady-state polarization curves in an operating polymer electrolyte fuel cell (PEMFC) showed that these electrocatalysts are active toward the ethanol oxidation reaction (EOR). The Ln-containing electrocatalysts exhibited ca. 225 mV more overpotential than Pt–Ru at a given current density based on the total electrocatalyst surface area in the anode, but this may be due to issues with particle size and electrode structure. Pt/C electrocatalysts containing Pr_6O_{11} nanorods were successfully prepared by Wang et al. [21] They observed that the Pr_6O_{11} nanorods have a supporting role for ethanol electro-oxidation on Pt/C. The promoting effect of Pr_6O_{11}, however, does not result from the easier electro-oxidation of the intermediate adsorbate on Pt–Pr_6O_{11}/C than on Pt/C. They supposed that Pr_6O_{11} could promote a certain step in ethanol oxidation, and that the special morphology of the nanorods could further enhance the activity compared with nanoparticles.

In our previous work [22], Pt–Pr/C electrocatalysts were prepared by a modified formic acid method and tested for carbon monoxide and ethanol oxidation in acid medium by CO stripping and linear voltammetry. The addition of Pr increased the electrocatalytic activity of Pt for both CO and CH_3CH_2OH oxidation. The enhanced activity of Pt–Pr/C catalysts was ascribed to both an electronic effect, by the presence of Pr_2O_3, and the bi-functional mechanism, by PrO_2 presence. The short-term stability and durability of these catalysts, however, were not evaluated. Short-term stability can be defined as the ability to recover activity lost during continuous operation. The catalytic activity decay is always concerned with operating conditions (such as poisoning by fuel contaminants or intermediate species by fuel cell reactions) and reversible material changes. Short-term stability is an important parameter to evaluate the effectiveness of supported catalysts. Chronoamperometric (CA) experiments are widely applied to explore the catalytic stability of fuel cell catalysts. Durability of a catalyst is its ability to resist permanent change in performance over time. Durability decay leads to a decrease in performance that is not recoverable or reversible (*i.e.*, due to loss of electrochemical surface area, loss of co-catalyst, carbon corrosion, etc.). This issue is related to ageing. Long-term structural durability of the catalysts is one of the characteristics most necessary for fuel cells to be accepted as a viable product. The electrochemically active surface area loss and electro-catalytic activity decrease of fuel cell catalysts are evaluated by various durability tests, mainly by repetitive potential cycling (RPC). In this work Pt–Pr/C electrocatalysts (Pt:Pr atomic ratio 9:1, 1:1 and 2:3) were prepared by a modified formic acid method, by reduction of metal precursors in CO atmosphere at 80 °C for 30 min. The metal precursors were simultaneously added to carbon support at an addition time of 40 min. The Pt–Pr/C (1:1) catalyst was also synthesized at different metal precursors addition times (MPAT) of 5, 15 and 40 min. For comparison the Pt–Pr/C (1:1) was also synthesized in H_2 atmosphere. Electrochemical techniques such as CO stripping, linear scan and derivative voltammetries along with chronoamperometry were employed to evaluate the EOR activity, short-term stability and durability of carbon supported Pt–Pr catalysts. Their electrochemical properties were compared with those of commercial Pt/C and Pt–Sn/C (3:1) catalysts.

2. Experimental section

2.1. Catalysts preparation

Pt–Pr/C catalysts were obtained by a modified formic acid procedure. The methodology was adding carbon Vulcan® in 0.5 mol L^{-1} of formic acid (Sigma Aldrich; 98.0%) on pH adjusted to 12.5 and heat the mixture at 80 °C in a reducing atmosphere gas. Two atmospheres were tested: hydrogen gas (H_2) and carbon monoxide (CO). An solution of $H_2PtCl_6.6H_2O$ (Alfa Aesar, 99.9%) and $PrCl_3$ (Sigma Aldrich, 34.0 wt% Pr). The precursor solution was added in an interval of 40 min. After the addition, the time of reaction was 30 min. The supported catalysts thus formed were filtered, washed with ultrapure water and dried at 80 °C for 2 h. Catalysts were prepared with a ratio of 20 wt% of metal on carbon. Three reasons metallic atomic PtPr were synthesized: 9:1, 1:1 and 2:3.

The time addition influence was valued on the Pt–Pr/C 1:1 characteristics catalyst. The addition time of precursors were programed by 5 min and 15 min. It was hoped 30 min after the addition of precursors, in a CO atmosphere. The obtained material was filtered and dried in an oven at 80 °C for 2 h.

2.2. Electrochemical measurements

The general electrochemical behaviour was characterized by cyclic voltammetry in 0.5 mol L^{-1} H_2SO_4, and the electro-catalytic activity towards ethanol oxidation was evaluated in 0.5 mol L^{-1} ethanol acid solution by linear sweep voltammetry (LSV) and chronoamperometry. All experiments were done at 25 °C in Ar saturated solutions. CO stripping experiments were carried out in the following way: after recording a cyclic voltammetry curve in an Ar purged system, CO was admitted to the cell and adsorbed at 0.1 V *vs.* RHE for 5 min. The excess CO was eliminated by passing Ar gas during 25 min and the adsorbed CO was oxidized at a scan rate of 5 mV s^{-1}.

Repetitive potential cycling (RPC) between 0.5 V and 1.0 V, at 50 mV s^{-1} for 200 cycles was carried out under Ar atmosphere. At intervals of 25 cycles, 3 cycles was carried out in the range of 0.05 V to 0.8 V. RPC between 0.05 V and 1.0 V, at 20 mV s^{-1} for 70 cycles was also carried out under CO atmosphere. For evaluation of activity area changes, CO stripping measurements were done before and after the RCP experiments.

All electrochemical measurements were done in a conventional electrochemical cell, with a Pt wire counter-electrode and a reversible hydrogen reference electrode.

The Pt–Pr electrocatalysts were used as ultra-thin layers. The materials were dispersed in 1.0 mL de 2-propanol and 15 μL 6.0 wt% Nafion suspension in alcoholic solution (DuPont, USA) to form electrocatalyst ink, that was deposited on a glassy carbon disk electrode (0.385 cm^2) previously polished down to alumina. In all cases, the catalysts layers had a metal (Pt + Pr) load of 28 μg cm^{-2}. A Pt/C and Pt–Sn/C (3:1) commercial catalyst (E-TEK) was used as reference sample. Solutions were prepared from analytical grade H_2SO_4 (Sigma Adrich), analytical grade ethanol (J.T. Baker) and ultra-pure water (MilliQ, Millipore).

3. Results

3.1. Electrochemical activity of Pt–Pr/C catalysts for CO and ethanol oxidation

The chemical and physical characteristics, that are EDX and XPS composition, lattice parameter and crystallite size by XRD, and particle size by TEM of Pt–Pr/C (Pt:Pr atomic ratio 9:1, 1:1 and 2:3) catalysts synthesized in CO atmosphere at a metal precursor addition time of 40 min, of Pt–Pr/C (1:1) synthesized in CO atmosphere at a metal precursor addition time of 5 and 15 min, and of Pt–Pr/C (1:1) synthesized in H_2 atmosphere at a metal precursor addition time of 40 min are shown in Table 1 from Ref. [22]. The lattice parameter and crystallite size of Pt/C and Pt–Sn/C (3:1) by E-TEK are also reported for comparison. The Pt–Sn/C (3:1) catalyst

by E-TEK was fully alloyed and constituted of the Pt_3Sn phase only. [23] As reported in Ref. [22], the shift of the onset of CO oxidation at lower potentials for all Pt–Pr/C catalysts observed in CO stripping voltammetry indicated the ability of Pr to promote the electro-oxidation of adsorbed CO. Whereas in Pt/C only one peak for CO oxidation is present, with a maximum at about 785 mV, in Pt–Pr/C catalysts, excluding the Pt–Pr/C (1:1) catalysts prepared at a MPAT of 40 min, two or three CO oxidation peaks are observed. The potential at the maximum of a CO oxidation peak was only slightly shifted with respect to that of Pt, and was in the range from 745 to 785 mV (named peak 1). The potential shift at the maximum of peak 1 was associated to an electronic effect of Pr_2O_3 on the adsorption/desorption of CO/CO_2 on Pt. The potential at the maximum of another CO oxidation peak was in the range 680–720 mV (named peak 2), and was associated to PrO_2 presence. The oxidation of adsorbed CO is facilitated by the presence of PrO_2, a strong oxidant agent, supplying oxygen atoms at an adjacent site at a lower potential than that accomplished by pure Pt. A third CO oxidation peak was present only on the Pt–Pr/C (9:1) with a maximum at about 500 mV (named peak 3). The small peak 3, present at low potential as a shoulder of peak 2, should be associated to the presence of a small amount of a $PtPr_x$ phase, such as Pt_3Pr. In the same way than Pt_3Sn, Pt_3Pr could induce the formation of weakly adsorbed CO sites, giving rise to CO oxidation at low potential. The electrochemically active surface areas (ECSAs) of Pt–Pr/C and commercial Pt–Sn/C and Pt/C catalysts were estimated from the CO_{ad} oxidation charge and reported in Table 2.

The electrochemical activity for the ethanol oxidation reaction of Pt–Pr/C, Pt–Sn/C and Pt/C catalysts was investigated by LSV measurements in H_2SO_4 solution at room temperature. As can be seen in Table 2, the ECSA normalized current density of all Pt–Pr/C catalysts was higher than that of Pt/C, and for the most part of Pt–Pr/C catalysts was also higher than that of Pt–Sn/C (3:1), and increased with increasing Pr content in the catalyst and with increasing MPAT. Derivative voltammetry (DV) represents the rate of change of voltammetric current i with respect to electrode potential $E(\partial i^{LSV}_{ECSA}/\partial E)$ and has more voltammetric features than conventional voltammogram. [24] For example, closely placed voltammetric peaks or shoulders can be resolved in derivative voltammograms, distinguishing ethanol oxidation peaks due to parallel path mechanisms peak in the forward scan. DVs of Pt–Pr/C and Pt/C catalysts obtained from the LSV curves reported in Fig. 1 from Ref. [22], with the addition of the DV of Pt–Sn/C, are shown in Fig. 2. DVs of Pt–Pr/C, Pt–Sn/C and Pt/C present multiple positive peaks, whereas the corresponding conventional voltammograms show only one peak with weak shoulders at the positive slopes. Ethanol oxidation on Pt, Pt–Ru and Pt–Sn occurs through parallel reaction pathways, related to intermediate species oxidation, depending on the potential and the metal added to Pt. [25–27] As in the case of Sn and Ru, also Pr does not improve C–C bond cleavage of Pt, [20] thus the main products of ethanol oxidation are acetaldehyde (AAL) and acetic acid (AA). There is a direct (analytical) evidence about the existence of the AAL and AA intermediates. Several studies on the electro-oxidation of ethanol have been devoted mainly to identifying the adsorbed intermediates on the Pt electrode and elucidating the reaction mechanism by means of various techniques, as differential electrochemical mass spectrometry (DEMS), in situ Fourier transform infrared spectroscopy (FTIRS) and electrochemical thermal desorption mass spectroscopy (ECTDMS) [26,28–32]. The global mechanism of ethanol oxidation in acid solution may be summarized in the following scheme of parallel reactions:

$$CH_3CH_2OH \rightarrow [CH_3CH_2OH]_{ad} \rightarrow C_{1ads}, C_{2ads} \rightarrow CO_2 \text{ (total oxidation)} \quad (1)$$

$$CH_3CH_2OH \rightarrow [CH_3CH_2OH]_{ad} \rightarrow CH_3CHO \rightarrow CH_3COOH \text{ (partial oxidation)} \quad (2)$$

The formation of CO_2 goes through two adsorbed intermediates C_{1ads} and C_{2ads}, representing fragments with one and two carbon atoms, respectively. Breaking the C–C bond for a total oxidation to CO_2 is a major problem in ethanol electrocatalysis. Thus, high yields of partial oxidation products, AAL and AA, are obtained at Pt catalysts [25,27]. On-line DEMS measurements showed that, in contrast

Table 2
ECSACO, current density at 0.6 V by LSV (jLSV0.6), steady state current density by CA (j_{ss}) and normalized j_{ss} by Pt mass fraction in the catalyst (j_{ss}/x^t_{Pt}) of Pt–Pr/C (Pt:Pr atomic ratio 9:1, 1:1 and 2:3) catalysts synthesized in CO atmosphere at a metal precursor addition time of 40 min, of Pt–Pr/C (1:1) synthesized in CO atmosphere at a metal precursor addition time of 5 and 15 min, and of Pt–Pr/C (1:1) synthesized in H_2 atmosphere at a metal precursor addition time of 40 min, and of Pt/C and Pt–Sn/C (3.1) by E-TEK.

Nominal comp. Pt:Pr	MPAT min	$ECSA_{CO}$ $m^2\ g_{Pt}^{-1}$	$(j^{0.6}_{LSV})$ μA cm^{-2}	j_{ss} μA cm^{-2}	(j_{ss}/x^t_{Pt}) μA cm^{-2}
9:1	40	30	96	60	67
1:1	40	30	121	63	114
2:3	40	47	134	64	133
1:1	15	52	83	44	77
1:1	5	72	64	51	94
1:1 (H_2)	40	32	62	55	96
Pt/C		62	42	53	53
Pt–Sn/C (3:1)		41	64	40	54

Table 1
EDX and XPS composition, lattice parameter and crystallite size by XRD, and particle size by TEM of Pt–Pr/C (Pt:Pr atomic ratio 9:1, 1:1 and 2:3) catalysts synthesized in CO atmosphere at a metal precursor addition time of 40 min, of Pt–Pr/C (1:1) synthesized in CO atmosphere at a metal precursor addition time of 5 and 15 min, and of Pt–Pr/C (1:1) synthesized in H_2 atmosphere at a metal precursor addition time of 40 min Ref. [22]. The lattice parameter and crystallite size of Pt/C and Pt–Sn/C (3:1) by E-TEK are also reported for comparison.

Nominal composition Pt:Pr	Metal precursor addition time min	EDX composition Pt:Pr/at%	Lattice parameter nm	Crystallite size by XRD nm	XPS composition Pt:Pr/at%	Pt (0), PrO_2 and Pr_2O_3 surface amount mol%			Particle size by TEM/nm	
						Pt (0)	PrO_2	Pr_2O_3	d_n	d_v
9:1	40	85:15	0.3909	8.3	86:14	67	35	51	6.5	8.9
1:1	40	47:53	0.3913	8.9	78:22	62	41	50	5.8	7.8
2:3	40	40:60	0.3911	6.0	81:19	55	31	50	4.6	5.7
1:1	15	49:51	0.3910	6.4	81:19	52	39	49	4.9	6.8
1:1	5	46:54	0.3909	4.8	79:21	50	31	52	2.6	3.5
1:1 (H_2)	40	49:51	0.3927	6.2	88:12	62	24	47	5.8	6.7
Pt/C			0.3921	2.3		60	35	51		
Pt–Sn/C (3:1)			0.4002[a]	4.1[a]					4.2[a]	

[a] Data from Ref. [23].

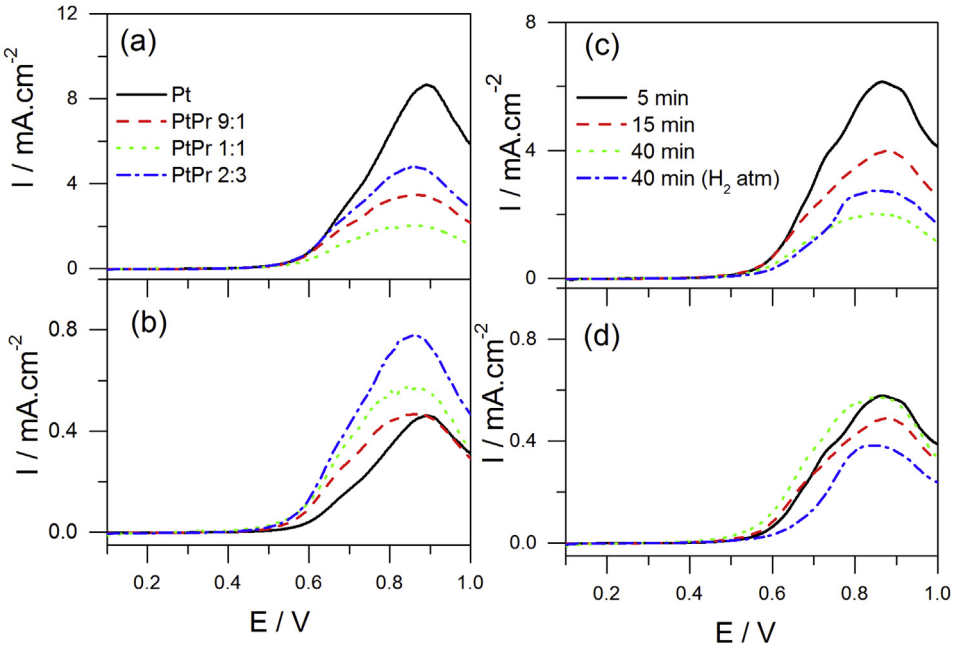

Fig. 1. Linear sweep voltammetry (LSV) measurements in 0.5 mol L^{-1} H_2SO_4 and 1.0 mol L^{-1} C_2H_5OH solution at room temperature for Pt–Pr/C electrocatalysts with various Pt:Pr atomic ratio, prepared in CO atmosphere at an MPAT of 40 min, and of the commercial Pt/C electrocatalyst (a and b), and for Pt–Pr/C (1:1) catalysts, prepared in CO atmosphere at different MPATs and prepared in H_2 atmosphere at an MPAT of 40 min (c and d), with the current density expressed in terms of the geometric surface area (a and c) and in terms of the $ECSA_{CO}$ area (b and d).
Reproduced from Ref. [22] with permission from PCCP Owner Societie.

to the higher EOR activity of the PtRu/C and Pt_3Sn/C catalysts with respect to Pt/C, the selectivity for complete ethanol oxidation to CO_2 is not enhanced significantly. Acetaldehyde and acetic acid were the major products for ethanol oxidation [33]. At 0.6 V, more acetic acid and less acetaldehyde was formed on the polyol-type Pt_3Sn/C and PtRu/C compared to the commercial catalysts. To oxidize acetaldehyde to acetic acid, oxygen species are needed. From the lower degree of alloying in the polyol-type Pt_3Sn/C or PtRu/C catalysts compared to the commercial ones it was concluded that the polyol-type catalysts contain more surface oxide species than their commercial counterparts, which would explain the more efficient further oxidation to acetic acid. Regarding the effect of rare earth addition on the EOR activity of Pt and ethanol oxidation products, by FTIRS measurements it was observed that the higher EOR currents on Pt–La (50:50) catalysts with respect to Pt are due to the formation of high amounts of acetic acid [34]. Analysis of the anode effluent with on-line gas chromatography showed that two-electron electro-oxidation of ethanol to acetaldehyde was the main reaction pathway at potentials of interest and implied that ethanol adsorbs without C–C bond cleavage through the oxygen in the hydroxyl group [20]. In this case AA behaves like a final product, while AAL can be a final products as well as an intermediate to be converted into AA, even in the presence of enhanced reaction activity due to Pr or Sn. It is known that the formation of AA and AAL takes place by different pathways [35–37]. For example, ethanol can be adsorbed dissociatively at platinum sites, either via an O-adsorption or a C-adsorption process, to form AAL species according to the following reactions: [35]

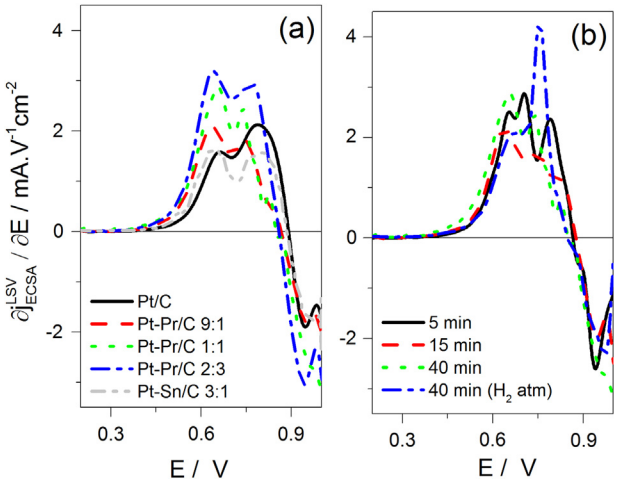

Fig. 2. Derivative of LSV curves from Ref. [22] ($\partial i^{LSV}_{ECSA}/\partial E$) *vs. E* plot for Pt–Pr/C electrocatalysts with various Pt:Pr atomic ratio, prepared in CO atmosphere at an MPAT of 40 min, and of the commercial Pt/C and Pt–Sn/C electrocatalysts (Fig. 1a), and for Pt–Pr/C (1:1) catalysts, prepared in CO atmosphere at different MPATs and prepared in H_2 atmosphere at an MPAT of 40 min (Fig. 1b).

$$Pt + CH_3{-}CH_2OH \rightarrow Pt{-}(OCH_2{-}CH_3)_{ads} + e^- + H^+ \quad (3)$$

or

$$Pt + CH_3{-}CH_2OH \rightarrow Pt{-}(CHOH{-}CH_3)_{ads} + e^- + H^+ \quad (4)$$

$$Pt{-}(OCH_2{-}CH_3)_{ads} \rightarrow Pt + CHO{-}CH_3 + e^- + H^+ \quad (5)$$

or

$$Pt{-}(CHOH{-}CH_3)_{ads} \rightarrow Pt + CHO{-}CH_3 + e^- + H^+ \quad (6)$$

These parallel processes of ethanol adsorption/AAL desorption occur at different potentials. As soon as AAL is formed, it can adsorb on platinum sites leading to a $Pt{-}CH_3{-}CO$ species:

$$Pt + CHO{-}CH_3 \rightarrow Pt{-}(CO{-}CH_3)_{ads} + H^+ + e^- \quad (7)$$

then, in the presence of a second metal M, such as Sn or Pr, because M is known to activate water at lower potentials than platinum, some OH species can be formed at low potentials on M sites according to reaction:

$$MO_x + H_2O \rightarrow MO_x{-}(OH)_{ads} + e^- + H^+ \quad (8)$$

and adsorbed acetaldehyde species can react with adsorbed OH species to produce acetic acid according to:

$$Pt{-}(CO{-}CH_3)_{ads} + MO_x{-}(OH)_{ads} \rightarrow Pt + MO_x + CH_3{-}COOH \quad (9)$$

As can be observed in Fig. 2, as in the case of methanol oxidation on Pt/C and Pt–Sn/C, [24] except the Pt–Pr/C (1:1) catalyst prepared in CO atmosphere at an MPAT of 5, which presents three intense peaks, two main positive peaks are present in the derivative voltammograms of ethanol oxidation on Pt–Pr, Pt–Sn and Pt catalysts, that is, a peak at higher potentials (named peak 1) in the range 740–755 mV for the Pr containing catalyst and at 788 mV for Pt/C and Pt–Sn/C catalysts, and a peak at lower potentials in the range 638–663 mV (named peak 2), both related to AA + AAL formation by different pathways, labelled as pathway 1 and pathway 2, respectively. Smaller peaks were present at potentials higher than 800 mV. The Pt–Pr/C (1:1) catalyst prepared in CO atmosphere at an MPAT of 5 min also presented a Pt-like peak at 790 mV and also an intense peak at an intermediate potential (704 mV). This anomalous behaviour with respect to the other Pt–Pr/C catalysts should be due to the short MPAT, causing weak interactions between Pr oxides and Pt. Being the anode potential for fuel cell application lower than 0.6 V *vs.* RHE, the pathway 2 is the most interesting. The shift to lower potentials of peak 1 maximum of Pt–Pr/C catalysts with respect to Pt/C is similar to the shift of peak 1 maximum observed in CO stripping measurements, and can be ascribed to an electronic effect, related to Pr_2O_3 presence. The peak 2 maximum of all Pt–Pr/C catalysts was higher than that of Pt and shifted to lower potentials, indicating the positive effect of PrO_2 on ethanol oxidation through pathway 2. Supposing that that the ethanol oxidation peaks relative to the different pathways are formed by the overlapping of the AAL and AA formation peaks, as can be seen in Fig. 3, and considering that OH species can be formed at low potentials on M sites according to reaction (8), enabling AA formation on Pt-M at lower potential than on pure Pt, on these bases $(\partial i^{LSV}_{ECSA}/\partial E)$ at the maximum peak increases in the presence of M, as indicated by the arrows in Fig. 3. This can explain the higher peak 2 maximum of Pt–Pr/C (and Pt–Sn/C) catalysts than that of Pt/C. The dependence of peak 2 to (peak 1 + peak 2) intensity ratio $(I_2/(I_1 + I_2))$ on $x^s_{PrO_2}$ is shown in Fig. 4.The value of $I_2/(I_1 + I_2)$ for the Pt–Pr/C (1:1) catalyst prepared under H_2 was lower than that of Pt/C. Indeed, in this catalyst a high Pr_2O_3 molar fraction (low $x^s_{PrO_2}$) gives rise to an increase of AAL + AA formation at higher potential by the electronic effect of Pr(3+) on Pt. The $I_2/(I_1 + I_2)$ ratio increased with increasing PrO_2 amount up to 40% $x^s_{PrO_2}$, which supports AA formation by the bi-functional mechanism: indeed, it is known that the addition of a second metal such as Sn to Pt, particularly in the oxide form increased not only the activity of the electrocatalyst and the electrical performance of the direct ethanol fuel cell (DEFC) but also changed the product distribution, favouring the formation of acetic acid [38]. For values of $x^s_{PrO_2} \geq 38\%$, the $I_2/(I_1 + I_2)$ ratio of Pt–Pr/C catalysts was higher than that of Pt–Sn/C. Above 40% $x^s_{PrO_2}$ the $I_2/(I_1 + I_2)$ ratio was almost constant. At the lower potential the dissociative adsorption of water on Pt is poor, thus the formation of AA through the pathway 2 is enhanced in the bimetallic catalysts. At the higher potential the dissociative adsorption of water is effective also on Pt, so the effect of the second metal is less important, and the oxidation of the ethanol and/or ethanolic residues can occur through oxygen transfer from a Pt–OH species.

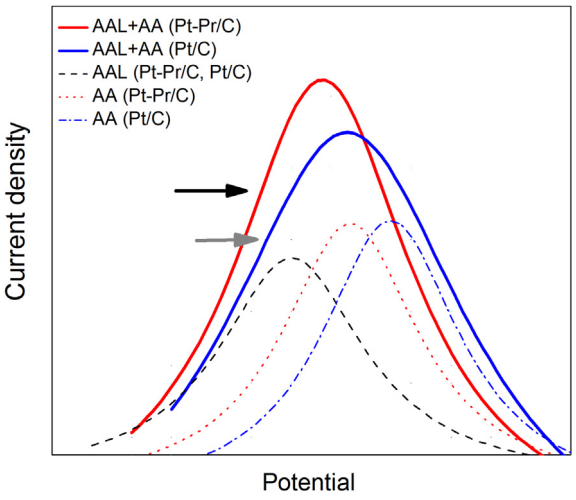

Fig. 3. Scheme of ethanol oxidation peak formation trough the pathway 2 in the i^{LSV} *vs.* *E* plot.

3.2. Short term stability

To evaluate both the electro-catalytic activity of the Pt–Pr/C catalysts in steady state conditions and the poisoning of the active surface, chronoamperometric experiments were carried out at 0.6 V in 0.5 M H_2SO_4 solution containing ethanol for 3600 s. The ECSA normalized current–time curves are shown in Fig. 5 for Pt–Pr/C catalysts with various Pr content, prepared in CO atmosphere at an MPAT of 40 min, and of the commercial Pt/C and Pt–Sn/C (3:1) catalysts (Fig. 5a), and for Pt–Pr/C (1:1) catalysts, prepared in CO atmosphere at different MPATs and prepared in H_2 atmosphere at an MPAT of 40 min (Fig. 5b). In all CA curves the current drops with time elapsing, rapidly at the beginning and then, also following a slight increase in some catalysts, such as Pt–Pr/C (2:3) and Pt/C, becomes relatively stable. The decay could be ascribed to poisoning

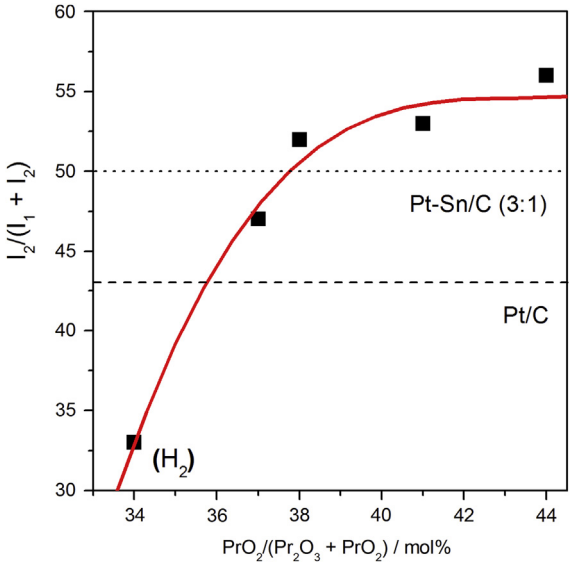

Fig. 4. Dependence of peak 2 to peak 1 + peak 2 intensity ratio $I_2/(I_1 + I_2)$ from derivative voltammograms of Pt–Pr/C on $x^s_{PrO_2}$. Dashed line: $I_2/(I_1 + I_2)$ of Pt(C; dotted line: $I_2/(I_1 + I_2)$ of Pt–Sn/C).

of surface active sites, assuming that initially the active sites are free from adsorbed ethanol molecules, but a new adsorption of ethanol molecules is a function of the liberation of the actives sites by adsorbed intermediate species (CO, CH_x, CH_3CHO and CH_3COOH) formed during the first period of time, which are responsible for poisoning of the catalytic sites. The poisoning of Pt–Pr/C and Pt–Sn/C catalysts was higher than that of Pt. The faster deactivation of Pt–Sn/C in comparison to Pt/C was also observed by Gupta et al. [39] and Beyan et al. [40] By CA measurements, they observed comparable catalytic activities for Pt and the Pt–Sn alloy electrodes in the initial current–time transient. However, over longer periods of time the activities of the Pt–Sn alloys diminish in comparison to Pt, providing evidence of the faster deactivation of the Pt–Sn electrodes. By comparing the steady state current density at 0.6 V *vs.* RHE by CA (j_{ss}) with the current density at 0.6 V *vs.* RHE by LSV ($j_{LSV}^{0.6}$) (see Table 2), it is evident that the poisoning of the Pt–Pr/C catalysts is higher than that of Pt/C. Indeed, conversely ($j_{LSV}^{0.6}$), the value of j_{ss} of all Pr containing catalysts is similar to that of Pt/C. However, taking into account of the overall Pt content in the catalyst, that is, dividing j_{ss} by Pt mass fraction in the catalyst (x_{pt}^{t}), the resulting Pt normalized steady state current density values of Pt–Pr/C catalysts were higher than that of Pt/C (see Table 2), indicating a positive effect of Pr presence.

3.3. Durability

3.3.1. Repetitive potential cycling under Ar atmosphere

To evaluate their structural stability, Pt–Pr/C with different Pt:Pr atomic ratio, Pt/C and Pt–Sn (3:1) catalysts have been submitted to repetitive potential cycling (RPC) between 0.5 and 1.0 V, at 50 mV s^{-1} for 200 cycles under Ar atmosphere. Two important effect have been reported regarding the potential cycling of Pt-M (M = non-noble metal) catalysts [41]: 1) Pt and M dissolve and the "real" Pt surface area changes with cycling, and 2) potential cycling yields an "activated" catalyst, attributed to a cleaning of the electrode surface. A Pt enrichment on catalyst surface is associated with the potential cycling technique [42–44]. In most electrochemical works Pt surface enrichment is regarded in terms of dissolution of the less noble component of the alloy [42–44]. CV curves in acid medium of Pt–Pr/C, Pt–Sn/C and Pt/C catalysts obtained before and after RPC are shown in Fig. 6a. The peaks corresponding to hydrogen adsorption/desorption of Pt–Pr/C and Pt/C become more distinguishable after RPC. The slight increase in peak area (or peak heights) is due to either a slight roughening of the catalyst surface which undergoes slight Pt and PtO_x dissolution, a rearrangement of Pt surface atoms or a cleaning effect, giving rise to a slight increase in the ECSA. Conversely, the area of the Pt–Sn/C catalyst markedly increased following RPC. This increase of area is due to Pt enrichment on surface, related to a noticeable dissolution of Pt_3Sn alloy with reprecipitation of Pt but not Sn. The effect of RPC on the active area was evaluated also by CO stripping curves (Fig. 6b). The ECSAs by CO stripping of Pt/C and Pt–Pr/C catalysts were substantially stable, confirming the CV results. The onset potential for CO oxidation and the shape of the CO stripping curves of Pt–Pr/C (1:1) and (2:3) catalysts were also stable, indicating negligible Pr oxide dissolution and stable PrO_2/Pr_2O_3 mass ratio. However, a change in the shape of the CO stripping curve of the Pt–Pr/C (9:1) catalyst was observed: the peak 3 disappeared, likely by dissolution of Pt_3Pr alloy, analogously to Pt_3Sn alloy. The CO stripping curve of Pt–Sn/C showed a large increase of the surface area, in agreement with CV result, an increase of the onset potential and a sharpening of the peak with a shift of the maximum to higher potential, that is, the curve of Pt–Sn/C becomes similar to that of Pt/C, ascribed to a Pt enrichment on the catalyst surface by Pt_3Sn dissolution of the Pt_3Sn alloy, followed by reprecipitation of Pt, but not of Sn. The LSV curves of Pt–Pr/C catalysts with various Pr content and of Pt/C and Pt–Sn/C before and after RPC under Ar atmosphere are reported in Fig. 7a. Following RPC the difference between the curves of Pt–Pr/C catalysts and Pt/C decreased. The potential cycling improves the EOR activity of Pt/C but decreases the EOR activity of Pt–Pr/C and Pt–Sn/C catalysts. The rearrangement of Pt atoms on the catalyst surface following RPC, as indicated by CV results, enhances ethanol adsorption/dehydrogenation as well as hydrogen adsorption/desorption on platinum; on the other hand, likely it causes a decrease of the number Pt–Pr interactions, but not their characteristics, as indicated by the stability of the shape of CO stripping curves, giving rise to a decrease of EOR activity, particularly at high potentials. For potentials up to 0.6 V *vs.* RHE (inset of Fig. 7a), an improvement of ethanol oxidation after cycling was observed for the Pt/C and Pt–Sn/C, notwithstanding Sn loss, while the EOR activity of Pt–Pr/C (1:1) and (2:3) was substantially stable, and that of Pt–Pr/C (9:1) decrease due to Pt_3Pr alloy dissolution. The increase of the EOR activity of Pt–Sn/C after RPC at low current density is not surprising: indeed, as reported by Colmati et al., [23] at low current density the activity for ethanol oxidation of Pt–Sn/C catalysts is not correlated with the Sn content in the catalyst, but goes through a maximum. Sn alloyed supports the oxidation of intermediate species to AA, but has a negative effect on the ethanol adsorption. Thus the loss of part of Sn can result in an increase of activity for ethanol oxidation of Pt–Sn/C catalysts. The DV of LSV curves (Fig. 7b) confirms the positive effect of cycling on Pt/C (increase of peak 1 and peak 2 intensity), and a decrease of peak 1 and peak 2 intensity of Pt–Pr/C and Pt–Sn/C catalysts. It has to be remarked, however, that the I_2/I_1 peak

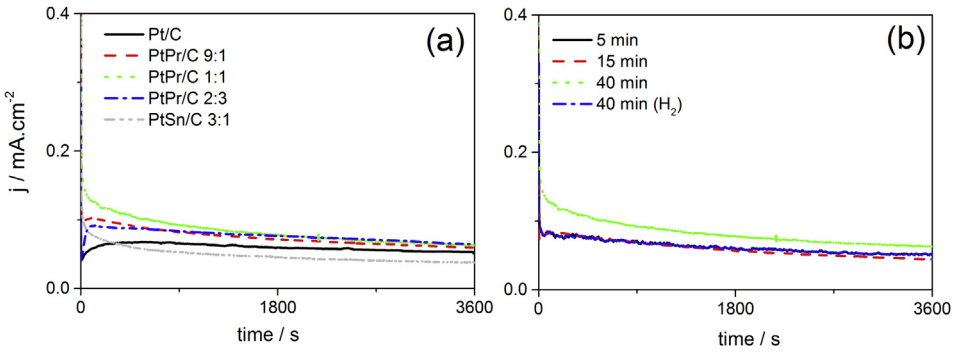

Fig. 5. ECSA normalized current–time curves for the different Pt-based electrocatalysts for different compositions, prepared in CO atmosphere at an MPAT of 40 min, and for commercial Pt/C and Pt–Sn/C (3:1) electrocatalysts (Fig. 4a), and for Pt–Pr/C (1:1) catalysts, prepared in CO atmosphere at different MPATs and prepared in H_2 atmosphere at an MPAT of 40 min (Fig. 4b).

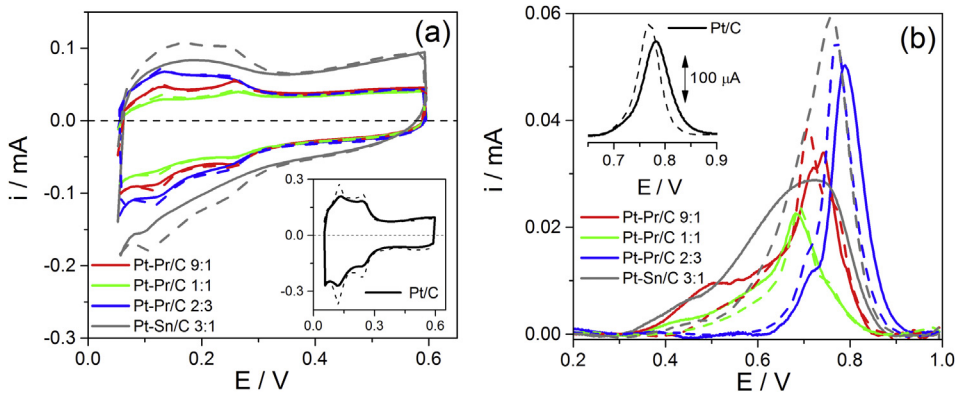

Fig. 6. CV curves in H_2SO_4 (Fig. 5a) and CO stripping curves (Fig. 5b) of Pt–Pr/C and commercial Pt/C and Pt–Sn/C catalysts before (full lines) and after (dashed lines) RPC under Ar atmosphere.

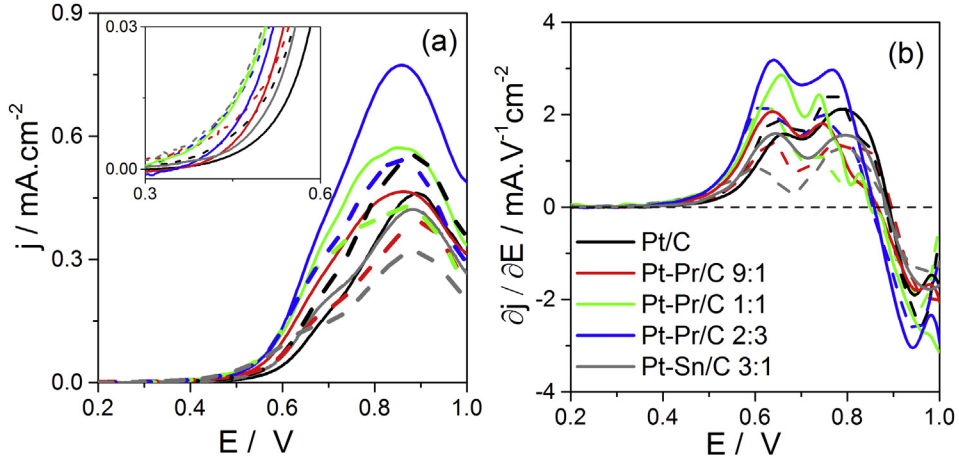

Fig. 7. LSV curve of Pt–Pr/C and commercial Pt/C and Pt–Sn/C catalysts (Fig. 6a), and the derivative of LSV curves ($\partial i_{ECSA}^{LSV}/\partial E$) *vs.* *E* plot (Fig. 6b) before (full lines) and after (dashed lines) RPC under Ar atmosphere.

intensity ratio of all Pt–Pr catalysts continued higher (with $I_2/I_1 > 1$) than the I_2/I_1 peak intensity ratio of Pt/C (with $I_2/I_1 < 1$), indicating the effect of PrO_2 presence also after RPC, while the I_2/I_1 peak intensity ratio of Pt–Sn/C goes from higher (before RPC) to lower (after RPC) than that of Pt/C, owing Sn loss from the catalyst surface.

3.3.2. *Repetitive potential cycling under CO atmosphere*

The Pt–Pr/C (1:1) prepared in CO atmosphere at an MPAT of 40 min, Pt–Sn/C (3:1) and Pt/C catalysts were also submitted to a short RPC (70 cycles) under CO atmosphere. CO stripping curves in acid medium of these catalysts before and after RPC under CO are shown in Fig. 8. A sharpening and a slight displacement towards more positive potential of CO stripping peak of Pt/C was observed. Shao-Horn et al. [45] found that the amount of defects (high index planes) decreased as a consequence of the RPC under CO. This affects CO oxidation, since it was reported that the reaction occurs at lower overpotentials in such defects rather than on terraces. [46] In the same way than following RPC under Ar atmosphere, also after RPC under CO atmosphere CO stripping curve of Pt–Sn/C showed a large increase of the surface area, an increase of the onset potential and a sharpening of the CO peak, more pronounced than after RPC under Ar atmosphere, ascribed to a Pt enrichment on the catalyst surface by Sn loss. Regarding the Pt–Pr/C catalyst, unlikely from RPC under Ar atmosphere, a remarkable shift of CO stripping peak was observed. On the basis of maximum peak potential, it can be inferred that a transition from peak 2 to peak 1 (see Section 3.1) occurred: considering that peak 2 is associated to PrO_2 presence and peak 1 is associated to Pr_2O_3, it can be supposed the loss of PrO_2 from the catalyst surface by the chemical reduction of almost all $Pr(4^+)$ to $Pr(3^+)$ and Pr(0) according to the following reaction:

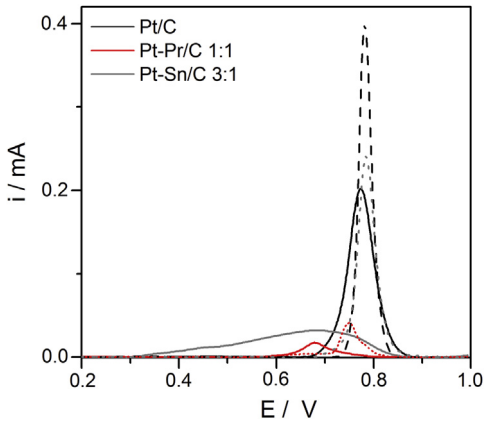

Fig. 8. CO stripping curves of Pt–Pr/C (1:1) prepared in CO atmosphere at an MPAT of 40 min, Pt–Sn/C (3:1) and Pt/C catalysts before (full lines) and after (dashed lines) RPC under CO atmosphere.

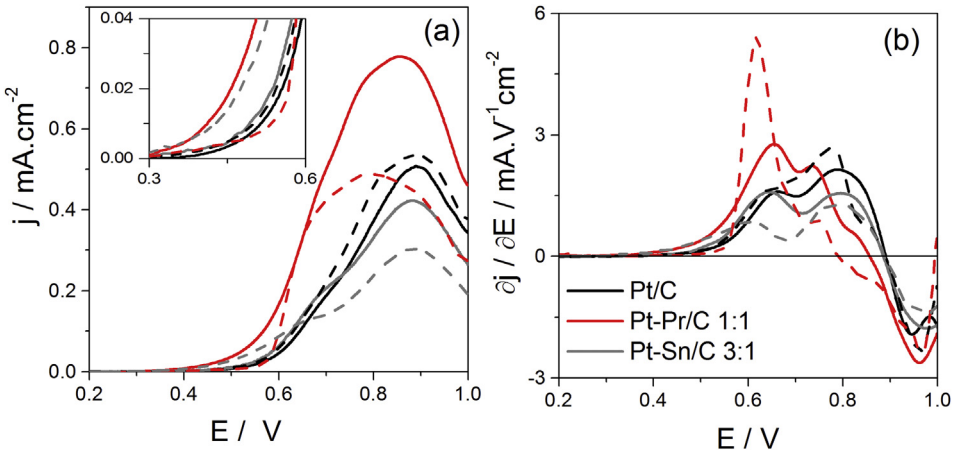

Fig. 9. LSV curve of Pt–Pr/C (1:1) prepared in CO atmosphere at an MPAT of 40 min, Pt–Sn/C (3:1) and Pt/C catalysts (Fig. 8a), and the derivative of LSV curves ($\partial i^{LSV}_{ECSA}/\partial E$) *vs.* *E* plot (Fig. 8b) before (full lines) and after (dashed lines) RPC under Ar atmosphere.

$$2\ PrO_2 + CO \rightarrow Pr_2O_3 + CO_2 \quad (10)$$

$$PrO_2 + 2\ CO \rightarrow Pr + 2\ CO_2 \quad (11)$$

Followed by the dissolution of Pr. By CO stripping measurements a large increase of the ECSA was also observed for the Pt–Pr/C catalyst. The increase in catalyst surface area could be ascribed to both a further surface segregation of Pt atoms by PrO_2 loss, as observed following RPC under CO atmosphere on Pt_3Co [47,48] and the change in the Pr-oxide structure. The LSV curves of Pt–Pr/C (1:1), Pt–Sn/C (3:1) and Pt/C catalysts before and after RPC under CO are reported in Fig. 9a. The Pt/C catalyst showed slightly better performance (slightly decrease of EOR onset potential and increase of current density at 0.6 V vs. RHE) due to Pt rearrangement on catalyst surface; instead the activity for ethanol oxidation of Pt–Pr/C was negatively affected by potential cycling under CO atmosphere: an increase of the EOR onset potential and a decrease the current density at 0.6 V *vs.* RHE (100 mA cm^{-2} *vs.* 121 mA cm^{-2}) was observed, due to the loss of the positive effect of PrO_2 on the ethanol oxidation reaction. The LSV curve of Pt–Sn/C was similar to that after RPC under Ar atmosphere. DV curves (Fig. 9b) indicated in the case of Pt/C negligible difference between before and after annealing; in the case of Pt–Sn/C DV was similar to that following RPC under Ar atmosphere. Conversely, for the Pt–Pr/C a large increase of peak 2 intensity, compared to untreated and submitted to RPC under Ar atmosphere Pt–Pr/C catalyst, was observed, likely related to an increase of AAL but not AA, because the reduction or absence of PrO_2, formation. Unlikely than Pt–Sn/C, following RPC both under Ar and under CO atmosphere the electrochemical features of the Pt–Pr/C catalyst doesn't become similar to Pt/C. The histogram in Fig. 10 shows the I_2/I_1 DV peak intensity ratio of Pt–Pr/C (1:1), Pt–Sn/C (3:1) and Pt/C catalysts before and after RPC in Ar and CO atmosphere. The histogram clearly shows the different effect of RPC on the mechanism for ethanol oxidation on Pt–Pr/C (1:1), Pt–Sn/C (3:1) and Pt/C catalysts. For the Pt–Pr/C catalyst the I_2/I_1 peak intensity ratio is always >1 and increase after RPC both under Ar and under CO atmosphere: RPC supports ethanol oxidation on Pt–Pr/C through pathway 2, markedly by RPC under CO atmosphere. Before cycling the I_2/I_1 ratio of Pt–Sn/C is ~1, and decreases following RPC: RPC decreases the ethanol oxidation on Pt–Sn/C through pathway 2, owing Sn loss, and the I_2/I_1 ratio of Pt–Sn/C becomes similar to Pt/C. Finally, the I_2/I_1 of Pt/C is always <1: RPC scarcely influences the mechanism of the EOR on Pt. Notwithstanding PrO_2 loss, as inferred by the change of CO stripping curve, pathway 2 is favoured, likely by supporting ethanol adsorption/dehydrogenation with AAL formation, not by AA formation. The very large I_2/I_1 peak intensity ratio after RPC under CO could be due to the formation of a core–shell structure with a Pt-rich shell [49–51], as suggested by the large increase of the ECSA by CO stripping, Such structural difference may have an influence on the ethanol oxidation reaction.

4. Conclusions

Carbon supported Pt–Pr catalysts were prepared by a modified formic acid method, and their electro-catalytic activity for ethanol oxidation, short-term stability and durability was compared with that of a commercial Pt–Sn/C (3.1) and Pt/C catalysts. Derivative voltammetry showed that ethanol electro-oxidation takes place by two main pathway at different potentials. The presence of a second metal supports the ethanol oxidation through the pathway at lower potential, which is the most interesting for fuel cell application. Short term stability tests indicated that Pt–Pr/C and Pt–Sn/C (3:1) catalysts were less tolerant to the poisoning by ethanol oxidation intermediate species than Pt/C. Durability test by repetitive potential cycling under Ar atmosphere revealed a good structural stability of Pt–Pr/C catalysts. The activity for ethanol oxidation was unchanged for potentials up to 0.6 V *vs.* RHE, but a slight decrease of

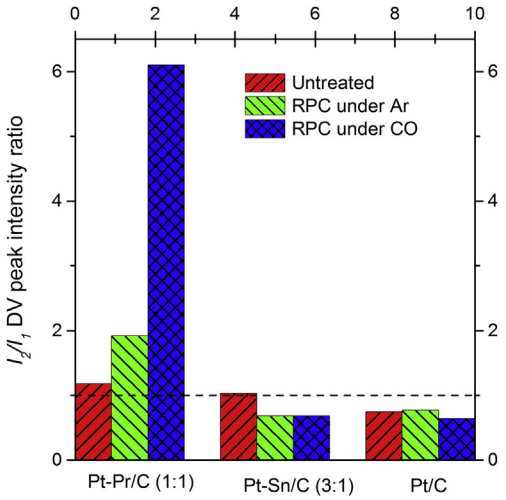

Fig. 10. Histogram of maximum I_2/I_1 DV peak ratio of Pt–Pr/C (1.1) and commercial Pt/C and Pt–Sn/C (3:1) catalysts before and after RPC in Ar and CO atmosphere.

the EOR activity was observed at higher potentials. On the other hand, Pt/C was stable and slightly improved its activity for ethanol oxidation, whereas Pt–Sn/C was not stable, suffering the dissolution of the Pt_3Sn alloy from the surface followed by reprecipitation of Pt, but not of Sn. Durability test by repetitive potential cycling under CO atmosphere carried out on Pt–Sn/C and Pt/C showed almost the same results than RPC under Ar atmosphere. The Pt–Pr/C (1:1), instead, exhibited a different behaviour than RPC under Ar atmosphere: PrO_2 loss or reduction to Pr_2O_3 was inferred by CO stripping measurements. An increase of the onset potential for CO and ethanol oxidation was observed. A large increase of DV peak 2 was also observed, likely by the increase of AAL formation. The large increase of the ECSA of Pt–Pr/C (1:1) suggested the formation of a core–shell structure with a Pt-rich shell.

Acknowledgements

The authors thank the grant 2010/20045-0 and 2012/12189-8, São Paulo Research Foundation (FAPESP) and thank CNPq (grant 307623/2012-2).

References

[1] E. Antolini, J. Perez, Int. J. Hydrogen Energy 36 (2011) 15752–15765.
[2] C.W. Xu, P.K. Shen, Chem. Commun. (2004) 2238–2239.
[3] C.W. Xu, R. Zeng, P.K. Shen, Z.D. Wei, Electrochim. Acta 51 (2005) 1031–1035.
[4] M.A. Scibioh, S.K. Kim, E.A. Cho, T.H. Lim, S.A. Hong, H.Y. Ha, Appl. Catal. B Environ. 84 (2008) 773–782.
[5] C.L. Campos, C. Roldan, M. Aponte, Y. Ishikawa, C.R. Cabrera, J. Electroanal. Chem. 581 (2005) 206–215.
[6] S.H. Bonilla, J.G.A. Carvalho, C.M.V.B. Almeida, B.F. Giannetti, C.F. Zinola, J. Electroanal. Chem. 617 (2008) 203–210.
[7] D.J. Diaz, N. Greenletch, A. Solanki, A. Karakoti, S. Seal, Catal. Lett. 119 (2007) 319–326.
[8] M. Takahashi, T. Mori, F. Ye, A. Vinu, H. Kobayashi, J. Drennan, J. Am. Ceram. Soc. 90 (2007) 1291–1294.
[9] J.S. Wang, X.Z. Deng, J.Y. Xi, L.Q. Chen, W.T. Zhu, X.P. Qiu, J. Power Sources 170 (2007) 297–302.
[10] J. Zhao, W.X. Chen, Y.F. Zheng, Mater. Chem. Phys. 113 (2009) 591–595.
[11] Y. Zhou, Y.F. Gao, Y.C. Liu, J.R. Liu, J. Power Sources 195 (2010) 1605–1609.
[12] D.M. Gu, Y.Y. Chu, Z.B. Wang, Z.Z. Jiang, G. Yin, Y. Liu, Appl. Catal. B Environ. 102 (2011) 9–18.
[13] Y.X. Bai, J.J. Wu, X.P. Qiu, J.Y. Xi, J.S. Wang, J.F. Li, W.T. Zhu, L.Q. Chen, Appl. Catal. B Environ. 73 (2007) 144–149.
[14] C.W. Xu, P.K. Shen, Y.L. Liu, J. Power Sources 164 (2007) 527–531.
[15] R.F.B. De Souza, A.E.A. Flausino, D.C. Rascio, R.T.S. Oliveira, E.T. Neto, M.L. Calegaro, M.C. Santos, Appl. Catal. B Environ. 91 (2009) 516–523.
[16] A.O. Neto, A.Y. Watanabe, R.M.D. Rodrigues, M. Linardi, C.A.L.G.O. Forbicini, E.V. Spinace, Ionics 14 (2008) 577–581.
[17] R.M.S. Rodrigues, M.M. Tusi, M.H. Chikasawa, C.A.L.G.O. Forbicini, M. Linardi, E.V. Spinace, A.O. Neto, Ionics 17 (2011) 189–193.
[18] M. Brandalise, M.M. Tusi, R.M.S. Rodrigues, E.V. Spinacé, A.O. Neto, Int. J. Electrochem. Sci. 5 (2010) 1879–1886.
[19] K. Asami, K. Kusakabe, N. Ashi, Y. Ohtsuka, Appl. Catal. A Gen. 156 (1997) 43–56.
[20] K.W. Lux, E.J. Cairns, J. Electrochem. Soc. 153 (2006) A1139–A1147.
[21] Y. Wang, T.S. Nguyen, C. Wang, X. Wang, Dalton Trans. (2009) 7606–7609.
[22] P.G. Corradini, E. Antolini, J. Perez, Phys. Chem. Chem. Phys. 15 (2013) 11730–11739.
[23] F. Colmati, E. Antolini, E.R. Gonalez, J. Electrochem. Soc. 154 (2007) B39–B47.
[24] A. Murthy, A. Manthiram, J. Phys. Chem. C 116 (2012) 3827–3832.
[25] S.C. Chang, L.W.H. Leung, M.J. Weaver, J. Phys. Chem. US 94 (1990) 6013–6021.
[26] H. Hitmi, E.M. Belgsir, J.M. Léger, C. Lamy, R.O. Lezna, Electrochim. Acta 39 (1994) 407–415.
[27] J.P.I. de Souza, S.L. Queiroz, K. Bergamaski, E.R. Gonzalez, F.C. Nart, J. Phys. Chem. B 106 (2002) 9825–9830.
[28] J. Willsau, J. Heitbaum, J. Electroanal. Chem. 194 (1985) 27–35.
[29] T. Iwasita, R. Dalbeck, E. Pastor, X. Xia, Electrochim. Acta 39 (1994) 1817–1823.
[30] B. Bittinscattaneo, S. Wilhelm, E. Cattaneo, H.W. Buschmann, W. Vielstich, Ber. Bunsen. Phys. Chem. 92 (1988) 1210–1218.
[31] V.M. Schmidt, R. Ianniello, E. Pastor, S. Gonzalez, J. Phys. Chem. US 100 (1996) 17901–17908.
[32] J.F.E. Gootzen, W. Visscher, J.A.R. vanVeen, Langmuir 12 (1996) 5076–5082.
[33] L. Colmenares, H. Wang, Z. Jusys, L. Jiang, S. Yan, G.Q. Sun, R.J. Behm, Electrochim. Acta 52 (2006) 221–233.
[34] T.A.B. Santoro, A. Oliveira Neto, C.A.L.G.O. Forbicini, M. Linardi, J.L. Rodriguez, E. Pastor, Int. J. Electrochem. 2012 (2012). ID 674150, 6.
[35] S. Rousseau, C. Coutanceau, C. Lamy, J.M. Leger, J. Power Sources 158 (2006) 18–24.
[36] H. Kim, S. Ho, J.L. Leighton, J. Am. Chem. Soc. 133 (2011) 6517–6520.
[37] M.H. Shao, R.R. Adzic, Electrochim. Acta 50 (2005) 2415–2422.
[38] R.M. Antoniassi, A. Oliveira Neto, M. Linardi, E.V. Spinacé, Int. J. Hydrogen Energy 38 (2013) 12069–12077.
[39] S. Sen Gupta, S. Singh, J. Datta, Mater. Chem. Phys. 116 (2009) 223–228.
[40] S. Beyhan, C. Coutanceau, J.M. Leger, T.W. Napporn, F. Kadirgan, Int. J. Hydrogen Energy 38 (2013) 6830–6841.
[41] K. Kinoshita, J. Lundquist, P. Stonehart, J. Electroanal. Chem. 48 (1973) 157–166.
[42] L.D. Burke, E.J.M. Osullivan, J. Electroanal. Chem. 112 (1980) 247–252.
[43] S.C. Zignani, E. Antolini, E.R. Gonzalez, J. Power Sources 182 (2008) 83–90.
[44] S.C. Zignani, E. Antolini, E.R. Gonzalez, J. Power Sources 191 (2009) 344–350.
[45] S.W. Lee, S.O. Chen, W.C. Sheng, N. Yabuuchi, Y.T. Kim, T. Mitani, E. Vescovo, Y. Shao-Horn, J. Am. Chem. Soc. 131 (2009) 15669–15677.
[46] N.P. Lebedeva, A. Rodes, J.M. Feliu, M.T.M. Koper, R.A. van Santen, J. Phys. Chem. B 106 (2002) 9863–9872.
[47] K.J.J. Mayrhofer, V. Juhart, K. Hartl, M. Hanzlik, M. Arenz, Angew. Chem. Int. Edit. 48 (2009) 3529–3531.
[48] E.G. Ciapina, E.A. Ticianelli, Electrochim. Acta 58 (2011) 172–178.
[49] P. Strasser, Rev. Chem. Eng. 25 (2009) 255–295.
[50] S. Papadimitriou, A. Tegou, E. Pavlidou, S. Armyanov, E. Valova, G. Kokkinidis, S. Sotiropoulos, Electrochim. Acta 53 (2008) 6559–6567.
[51] Y. Cai, R.R. Adzic, Ad. Phys. Chem. 2011 (2011). ID 50397, 16.